IOP Publishing | International Atomic Energy Agency Nuclear Fusion
Nucl. Fusion **55** (2015) 073020 (8pp) doi:10.1088/0029-5515/55/7/073020

Validation of comprehensive magnetohydrodynamic hybrid simulations for Alfvén eigenmode induced energetic particle transport in DIII-D plasmas

Y. Todo[1,2], M. A. Van Zeeland[3], A. Bierwage[4], W.W. Heidbrink[5] and M.E. Austin[6]

[1] National Institute for Fusion Science, Toki,Gifu 509-5292, Japan
[2] Department of Fusion Science, SOKENDAI (The Graduate University for Advanced Studies), Toki, Gifu 509-5292, Japan
[3] General Atomics, San Diego, CA 92186-5608, USA
[4] Japan Atomic Energy Agency, Rokkasho, Aomori 039-3212, Japan
[5] Department of Physics and Astronomy, University of California, Irvine, CA 92697, USA
[6] Institute for Fusion Studies, University of Texas at Austin, Austin, TX 78712 USA

E-mail: todo@nifs.ac.jp

Received 19 December 2014, revised 6 April 2015
Accepted for publication 13 May 2015
Published 19 June 2015

Abstract

A multi-phase simulation, which is a combination of classical simulation and hybrid simulation for energetic particles interacting with a magnetohydrodynamic (MHD) fluid including neutral beam injection, slowing-down, and pitch angle scattering, is applied to DIII-D discharge #142111 where the fast ion spatial profile is significantly flattened due to multiple Alfvén eigenmodes (AEs). The large fast ion pressure profile flattening observed experimentally is successfully reproduced by these first of a kind comprehensive simulations. Temperature fluctuations due to three of the dominant toroidal Alfvén eigenmodes in the simulation results are compared in detail with electron cyclotron emission measurements in the experiment. It is demonstrated that the temperature fluctuation profile and the phase profile are in very good agreement with the measurement, and the amplitude is also in agreement within a factor of two. This level of agreement validates the multi-phase hybrid simulation for the prediction of AE activity and alpha particle transport in burning plasmas.

Keywords: energetic particle, Alfvén eigenmode, hybrid simulation, magnetohydrodynamics

(Some figures may appear in colour only in the online journal)

1. Introduction

Alfvén eigenmodes (AEs) are one of the major concerns of burning plasmas because they can transport energetic alpha particles and reduce the alpha heating efficiency leading to deterioration of the plasma performance [1, 2]. In DIII-D experiments, significant flattening of the fast ion profile was observed during Alfvén eigenmode (AE) activity [3]. In the experiments, a rich spectrum of toroidal Alfvén eigenmodes (TAEs) and reversed shear Alfvén eigenmodes (RSAEs) driven by ∼80 keV neutral beam injection is observed during the current ramp-up phase with reversed magnetic shear. Many theoretical studies have been devoted to the DIII-D experiments, and they can be categorized into three groups, (1) studies of properties of AEs [4–8], (2) studies of fast ion transport and losses [9–11], and (3) nonlinear simulations [12–14]. For example, excellent agreement was found between ideal magnetohydrodymanic (MHD) NOVA predictions and electron cyclotron emission (ECE) measurements of the electron temperature fluctuation amplitude profile due to a TAE mode [4]. Fast ion induced shearing of 2-dimensional AE mode profile was measured by ECE imaging and well described by the gyrofluid-MHD hybrid code TAEFL [5]. It was demonstrated with the ORBIT simulation that multiple low-amplitude AE modes with $\delta B/B \sim O(10^{-4})$ can account for significant modification of fast ion distributions [9, 10]. The scintillator detector measurements of fast ion losses due to AE modes were reproduced with the ORBIT code [11].

Since the fast ion distribution in the DIII-D experiments is significantly affected by AEs, a comprehensive simulation, which deals with both the AEs and the fast ion transport as

self-consistently and realistically as possible, yet attainable on a tractable timescale, is needed. We have developed a multi-phase simulation, which is a combination of classical simulation and hybrid simulation for energetic particles interacting with an MHD fluid, in order to investigate a fast ion distribution formation process with beam injection, collisions, losses, and transport due to the AEs [15]. We use the MEGA code [16] for both the classical and hybrid simulations. We run alternately the classical simulation and the hybrid simulation in the multi-phase simulation. The code is run without MHD perturbations in the classical phase, while the interaction between the energetic particles and the MHD fluid is simulated in the hybrid phase. In the classical phase of the simulation, the fast ion distribution is built up with the beam injection and collisions. In the subsequent hybrid phase, the built-up fast ion distribution destabilizes AEs leading to the relaxation of the distribution. It was demonstrated with the multi-phase simulation that the fast ion spatial profile is significantly flattened due to the interaction with the multiple AEs with amplitude $\delta B/B \sim O(10^{-4})$, which is consistent with [9, 10] where resonance overlap of multiple AEs [17] was found to be the key mechanism for fast ion transport. The nonlinear MHD effects [18–22] that prevent the AE amplitude from growing up to large amplitude observed in a reduced simulation [23] are included in the hybrid simulation.

For the prediction of AE activity and energetic particle transport in burning plasmas, validation of simulations on the present experiments are important and indispensable. We have improved the simulation model from that used in [15] on two aspects; (1) we use an extended MHD model with thermal ion diamagnetic drift given in [24], and take account of the equilibrium toroidal flow; (2) we employ a more realistic beam deposition profile and power with the half and third beam energy components in addition to the full energy component. The total beam deposition power is increased to 6.25 MW from 4.95 MW used in [15]. With these improvements, we present the first comprehensive simulation that predicts both the nonlinear saturated amplitude of AEs and fast ion spatial profile consistent with measured values in experiment.

2. Simulation model

We use the MEGA code [16], in which the bulk plasma is described by the nonlinear MHD equations and the fast ions are simulated with the particle-in-cell method. Several hybrid simulation models have been constructed [16, 25–29] to study the evolution of Alfvén eigenmodes destabilized by energetic particles. In this work, we use an extended MHD model given in [24], and take account of the equilibrium toroidal flow. The extended MHD equations with the fast ion effects are given by

$$\frac{\partial \rho}{\partial t} = -\nabla\cdot(\rho\mathbf{v}_{\rm H}) + \nu_n\triangle(\rho-\rho_{\rm eq}), \tag{1}$$

$$\rho\frac{\partial}{\partial t}\mathbf{v} = -\rho\mathbf{v}_{\rm H}\cdot\nabla\mathbf{v} + \rho\mathbf{v}_{\rm pi}\cdot\nabla(v_\parallel\mathbf{b}) - \nabla p + (\mathbf{j}-\mathbf{j}_h')\times\mathbf{B} + \frac{4}{3}\nabla(\nu\rho\nabla\cdot\mathbf{v}) - \nabla\times(\nu\rho\boldsymbol{\omega}), \tag{2}$$

$$\frac{\partial p}{\partial t} = -\nabla\cdot[p(\mathbf{v}+\mathbf{v}_{\rm tor})] - (\gamma-1)p\nabla\cdot[\mathbf{v}+\mathbf{v}_{\rm tor}] + (\gamma-1)\left[\nu\rho\omega^2 + \frac{4}{3}\nu\rho(\nabla\cdot\mathbf{v})^2 + \eta\mathbf{j}\cdot(\mathbf{j}-\mathbf{j}_{\rm eq})\right] + \chi\triangle(p-p_{\rm eq}), \tag{3}$$

$$\frac{\partial\mathbf{B}}{\partial t} = -\nabla\times\mathbf{E},\ \mathbf{j} = \frac{1}{\mu_0}\nabla\times\mathbf{B}, \tag{4}$$

$$\mathbf{E} = -\mathbf{v}_E\times\mathbf{B} - \mathbf{v}_{\rm tor}\times(\mathbf{B}-\mathbf{B}_{\rm eq}) + \eta(\mathbf{j}-\mathbf{j}_{\rm eq}), \tag{5}$$

$$\mathbf{v}_{\rm H} = \mathbf{v} + \mathbf{v}_{\rm pi} + \mathbf{v}_{\rm tor},\ \mathbf{v}_{\rm pi} = -\frac{m_i}{2e_i\rho}\nabla\times\left(\frac{p\mathbf{b}}{B}\right), \tag{6}$$

$$v_\parallel = \mathbf{v}\cdot\mathbf{b},\ \mathbf{v}_E = \mathbf{v} - v_\parallel\mathbf{b},\ \boldsymbol{\omega} = \nabla\times\mathbf{v} \tag{7}$$

where μ_0 is the vacuum magnetic permeability, γ is the adiabatic constant, ν, ν_n and χ are artificial viscosity and diffusion coefficients chosen to maintain numerical stability. In this work, the dissipation coefficients ν, ν_n, χ, and η/μ_0 are assumed to be equal to each other. The dissipation terms play a physical role to enhance the damping of AE modes in the MHD simulation that does not include kinetic damping such as radiative damping [30] and thermal ion Landau damping. In this paper, we use one value of the coefficients, 5×10^{-7} normalized by $v_{\rm A}R_0$ where $v_{\rm A}$ is the Alfvén velocity at the plasma center, and R_0 is the major radius at the geometrical center of the simulation domain. The subscript 'eq' represents the equilibrium variables. The equilibrium toroidal flow velocity $\mathbf{v}_{\rm tor}$, which is assumed to be constant in time, and the thermal ion diamagnetic drift velocity $\mathbf{v}_{\rm pi}$ are included in the equations. For the thermal ion diamagnetic drift velocity given by equation (6), we retain only the magnetization current part and neglected the rest part that corresponds to the grad-B and curvature drift in order to keep the initial density profile in equilibrium. Otherwise, the density profile would evolve and deviate from the initial profile and become non-uniform on magnetic surface. The MHD momentum (equation (2)) includes the fast ion contribution in the fast ion current density $\mathbf{j}_h'$ that consists of the contributions from parallel velocity, magnetic curvature and gradient drifts, and magnetization current. The $\mathbf{E}\times\mathbf{B}$ drift disappears in $\mathbf{j}_h'$ due to the quasi-neutrality [16]. The fast ions are simulated using the full-f particle-in-cell (PIC) method, and a guiding-center approximation [31], where we employ the gyrokinetic approach to account for finite Larmor radius effects. The electromagnetic fluctuations are averaged over the fast ion gyro orbit for the fast ion dynamics. It was demonstrated that the MEGA code with the full-f PIC method can be applied to energetic particle modes in JT-60U, although the numerical noise level is higher in the full-f PIC simulation than in the delta-f PIC simulation [32, 33]. Cylindrical coordinates (R, φ, z) are used in the simulation. The numbers of grid points are (128, 128, 256) for (R, φ, z) coordinates, respectively. For the purpose of the data analysis, magnetic flux coordinates (r, φ, ϑ) were constructed for the MHD equilibrium where r is the radial coordinate with $r = 0$ at the plasma center and $r = a$ at the plasma edge, and ϑ is the poloidal angle.

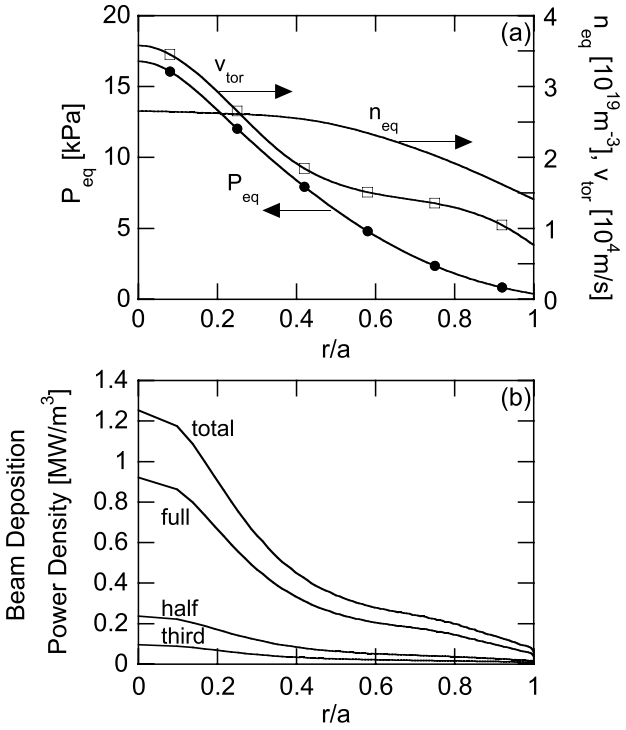

Figure 1. Equilibrium profiles of bulk pressure (p_{eq}), ion density (n_{eq}), and toroidal rotation velocity (v_{tor}); (a), and total beam deposition power profile with profiles for full, half, and third energy components; (b).

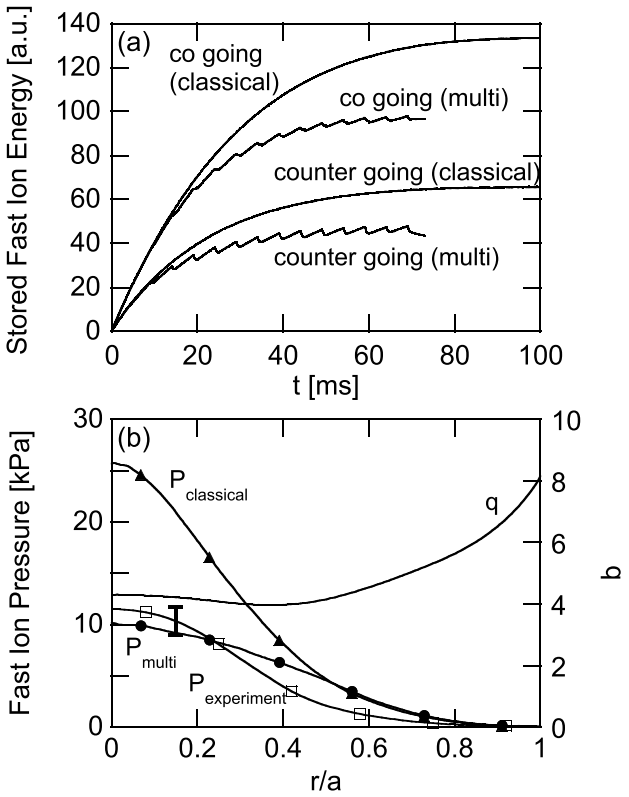

Figure 2. Time evolution of stored fast ion energy in multi-phase and classical simulations; (a), and comparison of fast ion pressure profile among multi-phase simulation (circle), classical simulation (triangle), and experiment (square) with an error bar shown in the figure; (b). The random error in the experimental fast-ion pressure associated with subtraction of the thermal pressure is represented by the error bar; the uncertainty in determination of the total pressure from equilibrium reconstructions contributes a comparable systematic error.

3. Simulation results and comparison with experiment

We have run a multi-phase simulation and a classical simulation for the DIII-D discharge #142111 at $t = 525$ ms. The equilibrium profiles of ion density ($n_{eq} = \rho_{eq}/m_D$), bulk pressure (p_{eq}), and toroidal flow velocity (v_{tor}), where m_D is deuterium mass, are shown in figure 1(a). We use experimental values for collision frequencies, the beam deposition power 6.25 MW (for the full, half, and third energy components). The beam deposition power profiles are shown in figure 1(b). 8 million computational particles are injected at a constant rate over a 150 ms time interval, although both the multi-phase and classical simulations are terminated before $t = 150$ ms. It was confirmed in a reduced simulation of bursting evolution of five AEs with toroidal mode number $n = 1$–5 that 2 million particles are sufficient for numerical convergence in burst interval, modulation depth of the stored fast ion energy at each burst, and saturation level of the stored fast ion energy [23]. We restrict the toroidal mode number of energetic particle drive in the simulation to $n = 1$–5 in order to reduce the numerical noise. This is supported by the experimental observation that the toroidal mode number of the AE modes is $n = 1$–5 at $t \sim 525$ ms [7]. Figure 2(a) shows the time evolution of stored fast ion energy. The multi-phase simulation was run with alternating classical phase for 4 ms and hybrid phase for 1 ms. This combination was repeated until stored fast ion energy is saturated at $t = 70$ ms, after which, the hybrid simulation was continuously run until $t = 72$ ms. Figure 2(b) compares the fast ion pressure profiles among the multi-phase simulation at $t = 72$ ms and the classical simulation at $t = 100$ ms, and the experiment. The fast ion pressure profile in the experiment is inferred from the Motional Stark Effect (MSE) constrained equilibrium reconstruction and the subtraction of the thermal pressure. We see in figure 2(b) that significant flattening of fast ion pressure profile takes place in the multi-phase simulation. The root-mean-square of the deviations from the experimental profile in $0 \leqslant r/a \leqslant 1$ is 1.36 kPa, which is 12% of the experimental central value and the same as the error bar shown in the figure. The multi-phase simulation gives the fast ion pressure profile closer to that in the experiment than our previous simulation with the same value of dissipation coeffcients 5×10^{-7} [15]. This is attributed to the beam deposition power (6.25 MW) with the full, half, and third energy components employed in the present simulation is higher than that in the previous simulation (4.95 MW) where only the full energy component was considered.

Bulk temperature fluctuation spectra with toroidal mode number $n = 1$–5 at $r/a = 0.49$ are shown for $t = 70$–72 ms in figure 3. The temperature fluctuation is normalized by the equilibrium temperature. The spatial profiles of the radial velocity and magnetic fluctuations are analysed for the highest peaks for $n = 2$–5, and a peak for $n = 1$ at 62 kHz, and are shown in figure 4. The spatial profiles consist of multiple poloidal harmonics, and are similar to those presented in figure 9 of [15], where the modes are identified as TAEs on

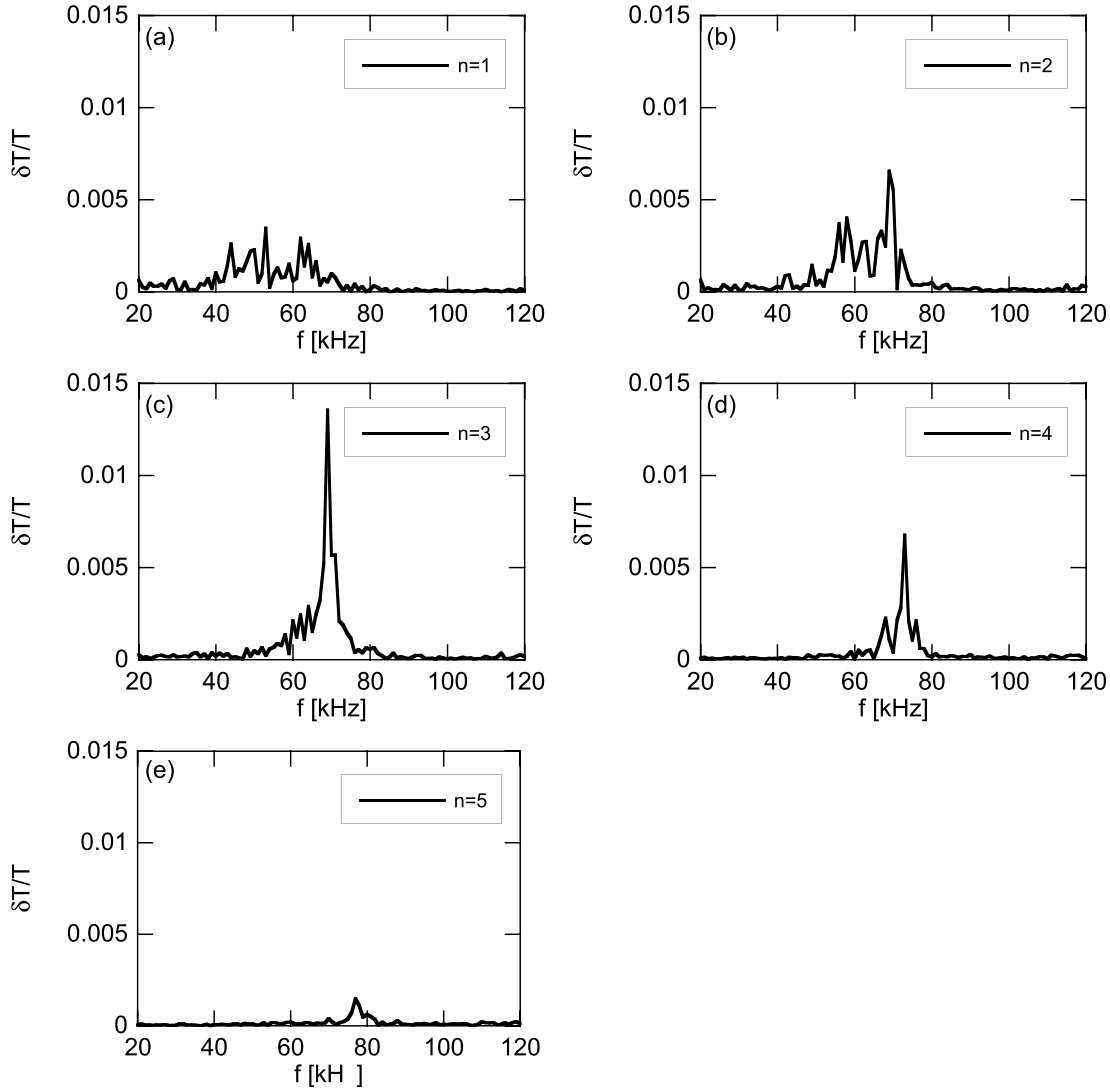

Figure 3. Frequency spectra of temperature fluctuation at $r/a = 0.49$ for 70.0 ms $\leqslant t \leqslant$ 72.0 ms for (a) $m/n = 4/1$, (b) $m/n = 8/2$, (c) $m/n = 12/3$, (d) $m/n = 16/4$, and (e) $m/n = 20/5$.

the basis of the spatial profiles and the comparison in frequency with the Alfvén continua. Then, we identify the modes shown in figure 4 as TAEs. The fluctuation amplitudes shown in figures 8, 9, 14, and 15(a) of [15] were doubled from the correct values by mistake. This mistake was corrected in the present work. At $t = 525$ ms in the experiment, the TAE modes with $n = 1$ and 3–5 are observed, whereas the $n = 2$ TAE mode is not. We should note that $n = 2$ modes are observed at other times in this discharge. The frequency of $n = 1$, and 3–5 modes is (simulation 62 kHz/experiment 68 kHz) for $n = 1$, (69 kHz/74 kHz) for $n = 3$, (73 kHz/79 kHz) for $n = 4$, and (77 kHz/84 kHz) for $n = 5$, respectively. We have agreement in frequency within 10%, which is better than our previous work where neither the thermal ion diamagnetic drift nor the equilibrium toroidal flow was considered. The thermal ion diamagnetic drift frequency and the equilibrium toroidal flow frequency are $4.0n$ kHz and $1.5n$ kHz, respectively, at $r/a = 0.49$. The TAE frequency is raised by the toroidal flow frequency and the half of the thermal ion diamagnetic drift frequency. The frequency in the present simulation is still lower than that in the experiment. This difference can be partially attributed to lack of the fast ion diamagnetic drift in equation (2). The effect of fast ion diamagnetic drift is discussed in [8, 29]. We can expect rise in the TAE frequency by $3.0n$ kHz, if we include the fast ion diamagnetic drift frequency in equation (2). On the other hand, we would like to point out the fast ion density and the impurity density, neither of which is considered in equation (2), would reduce the TAE frequency. The sum of fast ion mass density and impurity mass density with the main species of carbon amounts to 10% of the total mass density. Then, this would reduce the TAE frequency by 5%. These two effects would make the TAE frequency in the simulation closer to that in the experiment.

Next, we compare the simulation results with the ECE measurements in the experiment assuming equal temperature for electron and ion in the simulation. The spatial profiles of the temperature fluctuation and the phase are analysed for the dominant frequency of toroidal mode numbers $n = 3, 4$ and 5. The 2-dimensional electron temperature fluctuation profiles are shown in figure 5. We see the shearing profiles similar

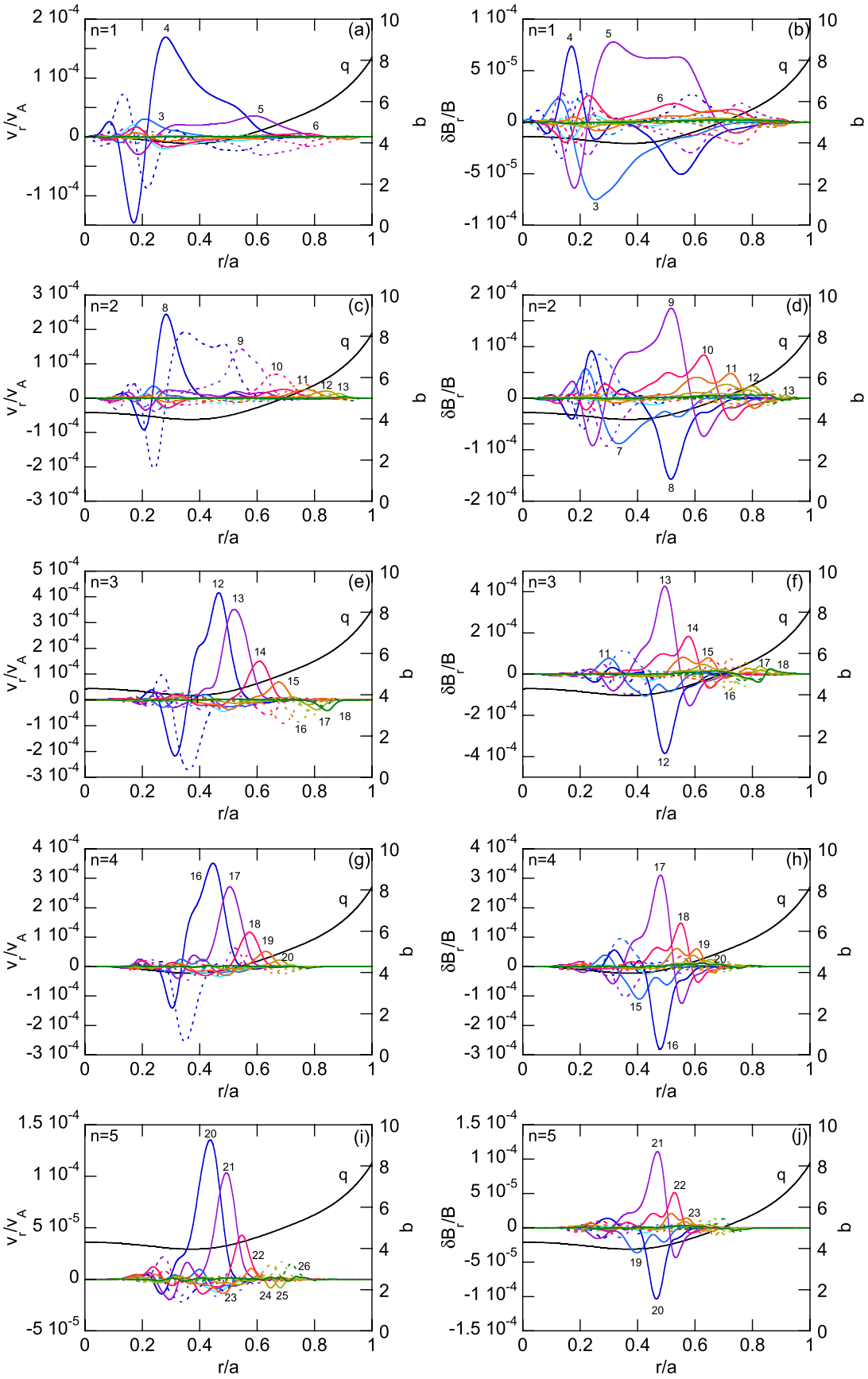

Figure 4. Radial velocity and magnetic fluctuation profiles of TAEs for 70.0 ms $\leqslant t \leqslant$ 72.0 ms with toroidal mode number and frequency (*a*), (*b*) $n = 1$, $f = 62$ kHz, (*c*), (*d*) $n = 2$, $f = 69$ kHz, (*e*), (*f*) $n = 3$, $f = 69$ kHz, (*g*), (*h*) $n = 4$, $f = 73$ kHz, (*i*), (*j*) $n = 5$, $f = 77$ kHz.

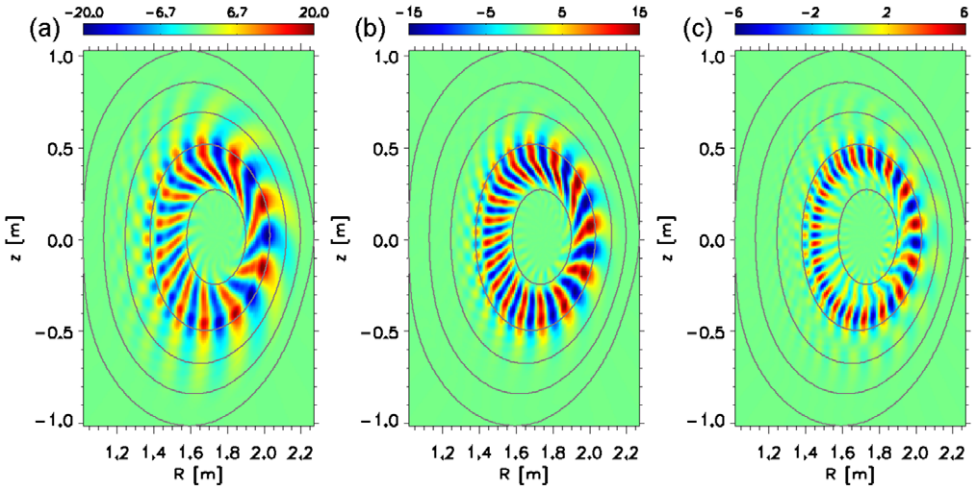

Figure 5. Electron temperature fluctuation profile in a poloidal plane (R, z) for (a) $n = 3$, $f = 69$ kHz, (b) $n = 4$, $f = 73$ kHz, and (c) $n = 5$, $f = 77$ kHz for 70.0 ms $\leqslant t \leqslant$ 72.0 ms.

to that discussed in [5]. The TAEs rotate in the clockwise direction in the figure. The tails of the fluctuation profile in the outer radius are leading the oscillation of the TAEs. In [5], the mode spatial profile without energetic particles is not shearing, and the shearing profile is attributed to the energetic particle effect. In our previous work [15], we performed simulations similar to the present simulation but without thermal ion diamagnetic drift and equilibrium toroidal flow. We found the shearing profile of the TAEs in the previous work. This is consistent with the conclusion of [5] that the shearing profile can be attributed to the energetic particle effect.

Figure 6 compares the electron temperature fluctuations for the $n = 3$–5 mode with those observed with the ECE measurements in the experiment. In figures 6(d)–(f), we see the phase ϕ in the experiment rises from the fluctuation peak locations at $r/a \sim 0.5$ towards the plasma edge, which indicate the shearing profiles. For quantitative comparison, we measure the following root-mean-square of deviations for amplitude (R_A) and phase (R_ϕ) over ECE measurement channels represented by i,

$$R_A = \left\{ \frac{1}{N} \sum_{i=1}^{N} \left[A\delta T_{e,\mathrm{sim}}(r_i - \alpha) - \delta T_{e,\mathrm{exp}}(r_i) \right]^2 \right\}^{1/2}, \qquad (8)$$

$$R_\phi = \left\{ \frac{1}{N_\phi} \sum_{i=\mathrm{i0}}^{\mathrm{i0}+N_\phi-1} \left[\phi_{\mathrm{sim}}(r_i) - \phi_0 - \phi_{\mathrm{exp}}(r_i) \right]^2 \right\}^{1/2}. \qquad (9)$$

For the comparison of amplitude, we find the optimum values of A and α that minimize R_A for the 18 channels shown in figure 6. The results are summarized in table 1. For the $n = 3$ mode, the optimum value $A = 1.01$ means that the absolute amplitude of the simulation is in very good agreement with the experiment. The deviation of the spatial profile is represented by R_A, which corresponds to 13% of the peak amplitude of the experiment. The optimum value of $\alpha = 0.03a$ indicates very good agreement in radial location. For $n = 4$ and 5, we see also good agreement for amplitude profile (R_A) and absolute amplitude (A). We see $\alpha = 0.08a$ for $n = 4$ and 5 for radial location. Since the magnetic shear is weak around $r/a = 0.5$, another equilibrium reconstruction with safety factor profile modified slightly within the experimental measurement error might lead to better agreement in radial location. For the comparison of phase, we find the optimum value of ϕ_0 that minimizes R_ϕ for the 8 channels at $0.4 < r/a < 0.8$. We do not include channels at $r/a < 0.4$ where the oscillation phase might be sensitive to a slight difference in q profile between simulation and experiment, because the rapid phase variation takes place at $r/a < 0.4$ in the simulation caused by the interaction with the continuum. Channels at $r/a > 0.8$ are also neglected because the fixed boundary condition employed in the simulation may affect the phase. For the $n = 3$ and 4 modes, we have a remarkable agreement in phase with $R_\phi/\pi = 0.06$. Also for the $n = 5$ mode with $R_\phi = 0.36$, we see good agreement for $0.3 < r/a < 0.6$ in figure 6(f).

4. Discussion and summary

In this paper, we presented new results of multi-phase simulation of DIII-D discharge #142111, where we use an extended MHD model with the thermal ion diamagnetic drift and the equilibrium toroidal flow, and we take account of the full, half, and third energy components of the injected beam. We have demonstrated that the fast ion spatial profile is significantly flattened due to the interaction with the multiple AEs and the fast ion pressure profile is in agreement with that of the experiment with the root-mean-square of the deviations same as the error bar. We quantitatively compared the predicted temperature fluctuation profiles of $n = 3, 4$, and 5 modes with ECE measurements, and it was found that the fluctuation profiles as well as phase profiles are in very good agreement with the measurements. Additionally, the saturated amplitudes are within a factor of 2 of those measured. We have improved the simulation model from that used in our previous work [15] with the extended MHD model and the half and third energy beam components. The extended MHD model with thermal ion diamagnetic drift and the equilibrium toroidal flow led to the better agreement in mode frequency with the experiment. The inclusion of the half and third energy beam components enhanced the total beam deposition power

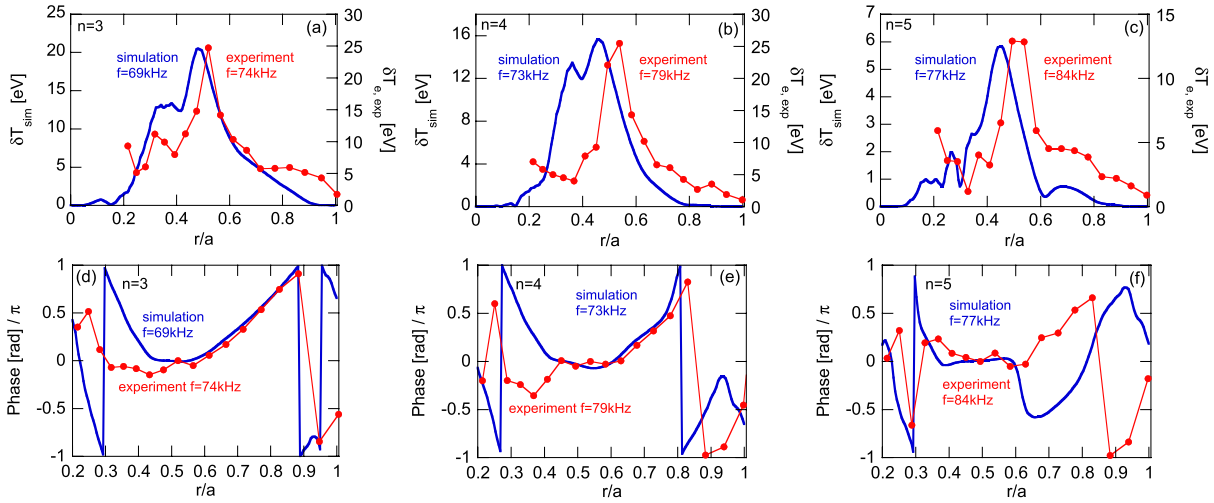

Figure 6. Comparison of electron temperature fluctuation profile for (*a*) $n = 3$, (*b*) $n = 4$, (*c*) $n = 5$, and the phase profile for (*d*) $n = 3$, (*e*) $n = 4$, (*f*) $n = 5$ between simulation and experiment. Left vertical axis is for simulation, while right for experiment in panels (*a*), (*b*), and (*c*).

Table 1. Quantification of electron temperature fluctuation profile comparison for (*a*) $n = 3$, (*b*) $n = 4$, (*c*) $n = 5$.

	A	α/a	R_A	R_ϕ/π
(*a*)	1.01	0.03	0.13	0.06
(*b*)	1.24	0.08	0.15	0.06
(*c*)	2.27	0.08	0.16	0.36

Note: R_A is normalized by the peak fluctuation level for each mode in the experiment. R_ϕ is measured for the 8 channels at $0.4 < r/a < 0.8$.

to 6.25 MW from 4.95 MW in the previous work, resulting in the better agreement in fast ion pressure profile with the experiment. We would like to emphasize that this validation exercise highlights the utility of our multi-phase simulation approach as a useful tool for the reliable prediction of AE activity and energetic particle transport in burning plasmas.

In this study, we assumed one value of the dissipation coefficients. As we discussed in our previous work [15], the dissipation coefficients enable us to control the damping rate, and we can adjust dissipation coefficients to match the experimental fast ion profile. We see in figure 12(*a*) in [15] another value of the coefficients 2×10^{-6} gives a fast ion profile close to that of the experiment, although the half and third beam energy components are not included. However, the coefficient value 5×10^{-7} gives amplitude of $n = 3$ and 4 modes close to those in the experiment, while the higher coefficient values result in lower amplitudes as we can know from the MHD kinetic energy shown in figure 12(*b*) of [15]. What is important is both the fast ion profile and the multiple AEs are well reproduced. In the present work, we found the fast ion profile is in agreement with that in the experiment for the coefficient value 5×10^{-7}, and confirmed the AE amplitudes are also in agreement within a factor of 2. The different level of agreement for the AE amplitudes shown in table 1 might be attributed to lack of kinetic damping in the present simulation model. For a perfect reproduction of all the AEs observed in the experiment, we need a more sophisticated simulation model that handles kinetic damping. On the other hand, the fast ion profile may not be sensitive to the individual damping rate of each mode in multi-mode systems.

Critical gradient models based on local linear stability analysis have been proposed [34, 35]. An advantage of these models is the kinetic damping mechanisms such as radiative damping and thermal ion Landau damping, which the simulation model of this work lacks. On the other hand, the present study has two important advantages. The first advantage is that the nonlinear MHD effects are retained. In [20, 22], it was found that both the zonal ($n = 0$) and higher-n nonlinear sidebands increase the damping rate of TAE. We found in the simulation presented in this paper that the zonal flow and field similar to those shown in figure 16 of [15] are generated. The damping rate enhanced by nonlinear sidebands will lead to a steeper spatial gradient than the linear analysis predicts. The second advantage is that the full phase space of fast ion is considered in the present study. This allows the fast ion distribution function to relax in velocity space in addition to position space. What is more important is that the degree of resonance overlap depends on the mode amplitudes. If the mode amplitudes are not large enough for the resonance overlap to cover the whole phase space, the fast ion flux may not be able to keep the fast ion distribution close to the marginal stability. There might be a gap between the linear marginal stability and the stiff profile where the resonance overlap covers the whole phase space and makes the profile resilient.

In our previous work [15], we performed multi-phase simulations with different classical phase duration (4 ms and 9 ms) and found good agreement between the two cases. From this, we concluded that if an entirely hybrid simulation was possible on a reasonable timescale, the results would be similar, i.e. a significant flattening of fast ion profile for relatively low AE amplitudes. We conjecture there would be limits for the period and interval of Alfvén physics application. The period of Alfvén physics(= 1 ms in our simulation) should be long enough for AEs to reach steady amplitude. We regard this as the time it takes to have the fast ion distribution well scrambled by AEs. The interval should be short enough for each fast ion not to miss any resonance with AEs in its life,

which is a slowing down process. During the slowing down process from the injection velocity to the thermal velocity, fast ions encounter multiple resonances with AEs. The interval of Alfvén physics application should be limited so that fast ions do not miss the resonances. The resonance regions have finite width for finite AE amplitude. Since the interval of Alfvén physics application is a few percent of the slowing down time (∼200 ms), we can expect that the multi-phase hybrid simulation gives a robust result for fast ion distribution, if the resonance regions have width of a few percent of the beam injection velocity.

Acknowledgments

Numerical computations were performed at the Helios of the International Fusion Energy Center, the Plasma Simulator of National Institute for Fusion Science, and the K Computer of RIKEN Advanced Institute for Computational Science (Project ID: hp120212). This work was partly supported by the JSPS-NRF-NSFC A3 Foresight Program in the field of Plasma Physics (NRF: No. 2012K2A2A6000443, NSFC: No.11261140328).

References

[1] Fasoli A. *et al* 2007 *Nucl. Fusion* **47** S264
[2] Heidbrink W.W. 2008 *Phys. Plasmas* **15** 055501
[3] Heidbrink W.W. *et al* 2007 *Phys. Rev. Lett.* **99** 245002
[4] Van Zeeland M.A. *et al* 2009 *Nucl. Fusion* **49** 065003
[5] Tobias B.J. *et al* 2011 *Phys. Rev. Lett.* **106** 075003
[6] Spong D.A. *et al* 2012 *Phys. Plasmas* **19** 082511
[7] Van Zeeland M.A. *et al* 2012 *Nucl. Fusion* **52** 094023
[8] Wang Z. *et al* 2013 *Phys. Rev. Lett.* **111** 145003
[9] White R.B., Gorelenkov N., Heidbrink W.W. and Van Zeeland M.A. 2010 *Plasma Phys. Control. Fusion* **52** 045012
[10] White R.B., Gorelenkov N., Heidbrink W.W. and Van Zeeland M.A. 2010 *Phys. Plasmas* **17** 056107
[11] Van Zeeland M.A. *et al* 2011 *Phys. Plasmas* **18** 056114
[12] Vlad G. *et al* 2009 *Nucl. Fusion* **49** 075024
[13] Chen Y. *et al* 2013 *Phys. Plasmas* **20** 012109
[14] Spong D.A. 2014 *Plasma Fusion Res.* **9** 3403077
[15] Todo Y., Van Zeeland M.A., Bierwage A. and Heidbrink W. 2014 *Nucl. Fusion* **54** 104012
[16] Todo Y. and Sato T. 1998 *Phys. Plasmas* **5** 1321
[17] Berk H.L., Breizman B. and Pekker M.S. 1995 *Nucl. Fusion* **35** 1713
[18] Spong D.A., Carreras B.A. and Hedrick C.L. 1994 *Phys. Plasmas* **1** 1503
[19] Zonca F., Romanelli F., Vlad G. and Kar C. 1995 *Phys. Rev. Lett.* **74** 698
[20] Todo Y., Berk H.L. and Breizman B.N. 2010 *Nucl. Fusion* **50** 084016
[21] Todo Y., Berk H.L. and Breizman B.N. 2012 *Nucl. Fusion* **52** 033003
[22] Todo Y., Berk H.L. and Breizman B.N. 2012 *Nucl. Fusion* **52** 094018
[23] Todo Y., Berk H.L. and Breizman B.N. 2003 *Phys. Plasmas* **10** 2888
[24] Hazeltine R.D. and Meiss J.D. 1992 *Plasma Confinement* (Reading, MA: Addison-Wesley)
[25] Park W. *et al* 1992 *Phys. Fluids B: Plasma Phys.* **4** 2033
[26] Spong D.A., Carreras B.A. and Hedrick C.L. 1992 *Phys. Fluids B: Plasma Phys.* **4** 3316
[27] Todo Y., Sato T., Watanabe K., Watanabe T.H. and Horiuchi R. 1995 *Phys. Plasmas* **2** 2711
[28] Briguglio S., Vlad G., Zonca F. and Kar C. 1995 *Phys. Plasmas* **2** 3711
[29] Wang X., Zonca F. and Chen L. 2010 *Plasma Phys. Control. Fusion* **52** 115005
[30] Mett R.R. and Mahajan S.M. 1992 *Phys. Fluids B: Plasma Phys.* **4** 2885
[31] Littlejohn R.G. 1983 *J. Plasma Phys.* **29** 111
[32] Bierwage A., Shinohara K., Aiba N. and Todo Y. 2013 *Nucl. Fusion* **53** 073007
[33] Bierwage A., Todo Y., Aiba N. and Shinohara K. 2014 *Nucl. Fusion* **54** 104001
[34] Ghantous K., Gorelenkov N.N., Berk H.L., Heidbrink W.W. and Van Zeeland M.A. 2012 *Phys. Plasmas* **19** 092511
[35] Bass E.M. and Waltz R.E. 2013 *Phys. Plasmas* **20** 012508